Green Chemistry

PAPER

View Article Online
View Journal | View Issue

Cite this: *Green Chem.*, 2024, **26**, 2645

Missing-linker defects in a covalent organic framework photocatalyst for highly efficient synthesis of tetrahydroquinoline†

Yuling Zhao,* Kangna Zhang, Keping Zhu, Yaqin Zhao, Hanping Zhai and Jikuan Qiu *

Cyclization of *N*,*N*-dimethylanilines with maleimides to obtain tetrahydroquinoline heterocyclic compounds is an essential reaction in industry but it is usually catalyzed by noble-metal catalysts under harsh conditions. High-performance, metal-free, low-cost, stable porous photocatalysts can provide an efficient pathway for the green synthesis of tetrahydroquinolines. Herein, we present a unique imine-based covalent organic framework, COF-HNU30-10, with good stability and a high density of structural defects for the selective cyclization of *N*,*N*-dimethylanilines with maleimides. Experiments show that various tetrahydroquinolines can be quantitatively synthesized (yield > 99.9%) using COF-HNU30-10 as a catalyst under visible-light irradiation. Such a yield is significantly higher than that (yield of 49%) obtained using a non-defective COFHNU30-0 and even higher than that obtained with Pt and Ru-based heterogeneous catalysts. A mechanistic study reveals that the introduction of defects in the framework facilitates the charge transfer and separation states, thus resulting in an enhancement of photocatalytic activity. Moreover, COF-HNU30-10 achieved a benchmark balance between the photocatalytic performance, stability and cost-effectiveness for the quantitative synthesis of tetrahydroquinolines.

Received 23rd November 2023,
Accepted 9th January 2024

DOI: 10.1039/d3gc04566h

rsc.li/greenchem

Introduction

Tetrahydroquinolines,[1–3] a vital family of nitrogen-containing heterocyclic compounds, are widely found in natural products. Demonstrating excellent biological and physiological activities, they are significant for drug discovery and new product development. Well-known examples include the schistosomicidal drug oxamniquine, antiarrhythmic drug nicainoprol, and antibiotic virantmycin[4] (Scheme 1). To date, various methods for constructing tetrahydroquinoline linkages have been reported, including quinoline hydrogenation, catalytic cyclization,[5–7] and the Beckmann rearrangement. Among these, the oxidative coupling cyclization reaction (OCCR) of *N*,*N*-dimethylanilines with maleimides to prepare tetrahydroquinolines has received significant attention owing to its high conversion efficiency and wide substrate applicability.

Integrating photochemical reactions into OCCR allows the transformations to occur under mild conditions and provides an economically and environmentally attractive pathway to construct tetrahydroquinolines.[8–10] Various photocatalysts, such as metal complexes (including [TBA][Pt(CNC)TzR],[11] Ru

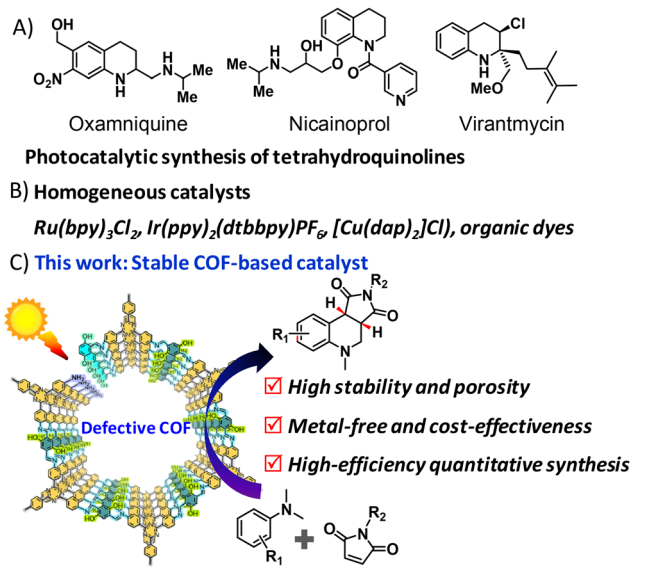

Scheme 1 (A) Representative examples of tetrahydroquinolines in biologically active molecules. (B and C) Different photocatalysts for the synthesis of tetrahydroquinolines.

Collaborative Innovation Center of Henan Province for Green Manufacturing of Fine Chemicals, School of Chemistry and Chemical Engineering, Key Laboratory of Green Chemical Media and Reactions, Ministry of Education, Henan Normal University, Xinxiang, Henan 453007, P. R. China. E-mail: qiujikuan@htu.edu.cn, ylzhao@htu.edu.cn

† Electronic supplementary information (ESI) available. See DOI: https://doi.org/10.1039/d3gc04566h

$(bpy)_3Cl_2$,[12] $Ir(ppy)_2(dtbbpy)PF_6$,[13] and $[Cu(dap)_2]Cl$)[14] and organic dyes[15] have been exploited for triggering OCCR of *N*,*N*-dimethylanilines with maleimides.[16–18] These catalysts with well-defined active centers exhibit high selectivity and activity. However, they are usually homogeneous, which would lead to the difficult recovery and reuse of these expensive catalysts after catalytic reactions. Thus, efforts have been devoted to constructing heterogeneous photocatalysts that are recyclable, reusable, cost-effective, and highly active.

Covalent organic frameworks (COFs),[19–22] an emerging class of crystalline, porous polymer materials, are constructed from molecular organic building units and joined by covalent bonds. Notably, the reticular chemistry of COFs with an ordered π-conjugated system allows accelerated migration of photogenerated charge carriers by channels and provides well-defined active sites for chemical reactions.[23–27] Hence, COFs have recently attracted much attention as novel semiconductor materials toward thermal catalysis and photocatalysis.[28–32] Relying on the favorable characteristics of controllable structure, regularity, and high stability, several COF-based photocatalysts have been applied to OCCR to prepare tetrahydroquinolines. For example, a Pt-loaded COF was used as a photocatalyst for oxidative cyclization, where the loaded Pt can enhance the photocatalytic activity of COFs.[33] In addition, a porphyrin-based COF was used as a metal-free heterogeneous photocatalyst for the initial synthesis of tetrahydroquinolines.[13] Based on these findings, the performance of COFs is either low or a noble metal is necessary to improve catalytic efficiency. Therefore, the exploration of metal-free and cost-effective COF photocatalysts to enhance OCCR performance is highly desirable, but equally challenging.

Inspired by previous works on maximizing semiconductor performance using defect engineering,[34,35] we present the fabrication process of COF-HNU30-10, a unique imine-based covalent organic framework characterized by good stability, a uniform spherical structure, and a controlled density of structural defects within the framework. The resultant COF was efficiently utilized as a metal-free heterogeneous catalyst for OCCR to prepare tetrahydroquinolines under visible-light irradiation. Compared to the non-defective COF-HNU30-0, the catalytic efficiency of COF-HNU30-10 increased by a factor of two, with the yield of the product increasing from 49% to >99.9% (Table 1, entries 10 and 11). Further characterization techniques revealed that the introduction of defects into the framework can greatly enhance the charge transfer and separation efficiency of photogenerated electron–hole pairs, thereby improving the photocatalytic activity. To the authors' knowledge, this is the first study that features a COF with structural defects triggering an OCCR for the quantitative synthesis of tetrahydroquinolines under visible-light irradiation.

Table 1 The optimization of reaction conditions for the photocatalytic synthesis of tetrachloroquinolines using COF-HNU30-*x*[a]

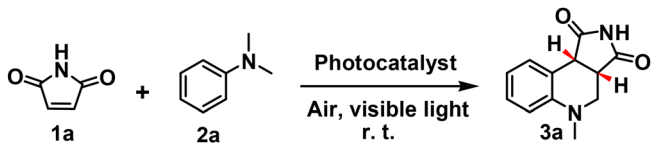

1a 2a 3a

Entry	Photocatalyst	Solvent	Time (h)	Yield[b] (%)
1	Catalyst-free	DMF	15	None
2	COF-HNU30-10	DMF	6	70
3	COF-HNU30-10	Acetonitrile	6	4
4	COF-HNU30-10	Dioxane	6	10
5	COF-HNU30-10	Ethanol	6	5
6	COF-HNU30-10	Methanol	6	9
7[c]	COF-HNU30-10	DMF	15	None
8[d]	COF-HNU30-10	DMF	15	None
9[e]	COF-HNU30-10	DMF	15	5
10	COF-HNU30-10	DMF	15	>99.9
11	COF-HNU30-0	DMF	15	49
12	COF-HNU30-5	DMF	15	75
13	COF-HNU30-20	DMF	15	90
14	COF-HNU30-30	DMF	15	60

[a] Reaction conditions: 0.25 mmol **1a**, 0.5 mmol **2a**, 5 mg COF-HNU30-*x*, 2 mL solvent, ambient air atmosphere, room temperature, and irradiation using a 20 W LED white light source. [b] NMR yields. [c] Under dark conditions. [d] Under a nitrogen atmosphere. [e] A 20 W blue light (410 nm) was used as the light source.

Results and discussion

We selected the low-cost monomers 2,4,6-tris(4-amino-phenyl)-1,3,5-triazine (TAPT), 2,5-dihydroxybenzaldehyde (Dhb), and 2,5-dihydroxyterephthalaldehyde (Dha) to synthesize a stable, highly porous, crystalline, and defect-rich COF (COF-HNU30-*x*, *x* = [Dhb]/[Dhb + Dha] × 100). As schematically depicted in Fig. 1A, different molar ratios (*x* = 0, 5, 10, 20, and 30) of mixed aldehydes and amine monomers were separately placed in glass beakers. The polymerization reaction was catalyzed by acetic acid at room temperature for 72 h (Fig. 1A and B, see the details in the ESI†). This method is also feasible for the gram-scale synthesis of highly crystalline defect-rich COFs. A similar method was adopted to obtain approximately 1 g of COF-HNU30-10 powder. Powder X-ray diffraction (PXRD) measurements of the powder confirmed the formation of highly crystalline COF materials (Fig. S1†). The Fourier-transform infrared (FTIR) spectrum of COF-HNU30-0 exhibited a strong absorption peak at 1575 cm^{-1}, corresponding to the stretching vibration of –C═N– (Fig. S2†), indicating that imine bonds were formed through the condensation of aldehydes with amines.[36]

The crystalline structure of COF-HNU30-*x* was analyzed using a PXRD analyzer. COF-HNU30-0 exhibited prominent diffraction peaks at 2θ = 2.8 and 5.0°, corresponding to the (100) and (110) reflection planes, indicating a high degree of crystallinity in the synthesized material (Fig. 1B). Simulation of the stacking model for COF-HNU30-0 performed using Materials Studio software indicated an overlapping AA stacking model structure (Fig. S3†). The PXRD results calculated from the AA stacking model were consistent with the experimental results. Furthermore, introducing a single aldehyde monomer into COF-HNU30-*x* significantly altered its crystallinity. In

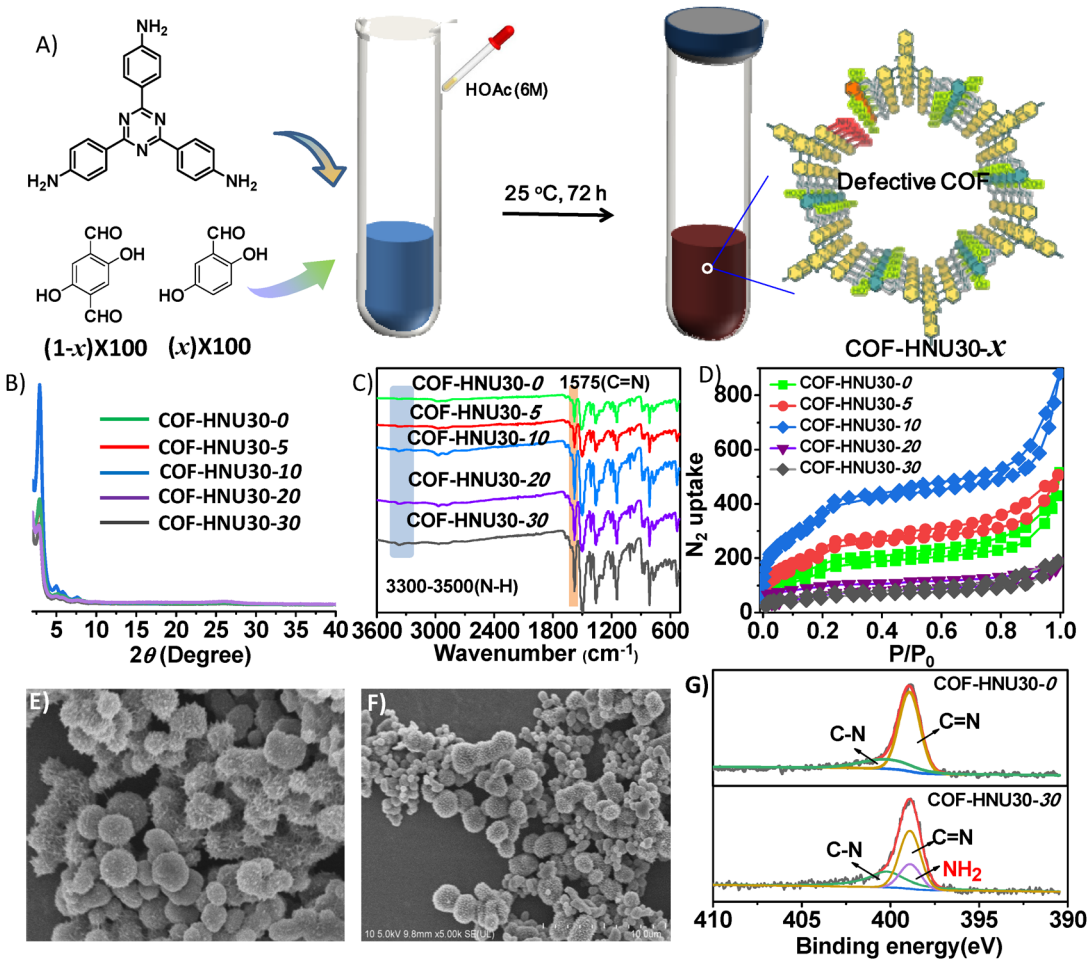

Fig. 1 (A) Schematic representation for the production process of defective COF-HNU30-*x*. (B–D) PXRD patterns, FTIR and N_2 sorption isotherms of COF-HNU30-*x*. (E and F) SEM images COF-HNU30-0 and COF-HNU30-30. (G) High-resolution XPS spectra of deconvoluted N 1s of COF-HNU30-0 and COF-HNU30-30.

comparison with COF-HNU30-0, higher sharp reflections were observed in COF-HNU30-5 and COFHNU30-10 (Fig. S4†), meaning that the addition of a single aldehyde monomer in the frameworks could efficiently improve its crystallinity. In contrast, COF-HNU30-20 and COF-HNU30-30 exhibited a weaker crystalline framework (Fig. S5†). This phenomenon may be caused by a partial structural collapse in the framework because more single aldehyde monomers will significantly block the periodicity of atomic structure arrangement in the COF.

The structural defects in COF-HNU30-*x* were confirmed using various techniques. Adding the monoaldehyde Dhb into the reaction system partially breaks the imine linkers, creating vacancy defects; thus, the unreacted amino groups were exposed as defect sites in the framework. The FTIR spectra of COF-HNU30-*x* (x = 5, 10, 20, and 30) show the corresponding characteristic stretching vibration bands of the N–H bond at 3300–3500 cm^{-1}, which belonged to the primary amino groups after adding Dhb (Fig. 1C). The intensity of these amino characteristic peaks increased after adding Dhb to the reaction system, verifying the successful generation of amino groups in the framework.[35] Scanning electron microscopy images revealed that the prepared COF-HNU30-0 exhibited a uniform spherical morphology with a particle size of 500 nanometers (Fig. 1E). The addition of Dhb to the reaction system resulted in the formation of two size-different spheres, with the proportion of smaller spheres in COF-HNU30-*x* increasing gradually with the increase of Dhb amount (Fig. 1F and Fig. S6–S9†). This result could be attributed to a structural collapse in COF-HNU30-*x*, thus resulting in a smaller diameter of the spherical structure. To further verify the partial conversion of imine linkers to amino groups, X-ray photoelectron spectroscopy (XPS) analyses were performed (Fig. 1G). The binding energy spectrum of N 1s of pristine COF-HNU30-0 exhibits two main peaks corresponding to C=N (398.9 eV) and C–N (400.2 eV). After defect engineering, a fraction of the N 1s peak shifts to a lower binding energy (398.8 eV), attributed to the decrease of the imine group and the new peak corresponds to the amino groups.[35] In addition, the percentage of amino groups in COF-HNU30-*x* (x = 5, 10, 20 and 30) was calculated by the

integration of the area of the peaks corresponding to the imine and amino groups to be 4.6%, 9.5%, 19.1, and 27.3%, respectively (Fig. S10–S14†).

The pore characteristics of COF-HNU30-*x* were analyzed using low-temperature N_2 adsorption–desorption measurements (Fig. 1D). All the synthesized COFs exhibited typical type IV adsorption isotherms, a characteristic of mesoporous materials.[37] The BET surface areas of COF-HNU30-*x* (*x* = 0, 5, 10, 20, and 30) were calculated as 582, 851, 1372, 250 and 208 $m^2\ g^{-1}$, respectively. The excessive number of defects in the framework reduces the surface area because of the partial structural collapse of COF-HNU30-20 and COF-HNU30-30. Moreover, COF-HNU30-*x* has good thermal and chemical stability. The four COFs exhibit high thermal stability up to 420 °C by thermogravimetric analysis (Fig. S15–S19†). After being immersed in different solvents for 3 days, the recovered COF-HNU30-*x* also maintained a highly crystalline structure (Fig. 2 and Fig. S20–S24†). The high chemical stability of COF-HNU30-10 can be attributed to the intramolecular hydrogen bond between O–H and C=N.[38]

Next, the catalytic activity of COF-HNU30-*x* was evaluated for the OCCR of *N*,*N*-dimethylanilines with maleimides to prepare tetrahydroquinolines under visible-light irradiation. *N*,*N*-Dimethylaniline (**1a**) and maleimide (**2a**) were initially selected as model substrates to explore the optimal reaction conditions in ambient air. As shown in Table 1, the reaction did not proceed smoothly without any catalyst under visible-light irradiation (Table 1, entry 1). The product yield strongly depended on the reaction medium (Table 1, entries 2–6). We observed that, under visible-light irradiation for 6 h, the best yield was obtained in DMF as the solvent (70%, entry 2). The yield was very low in the other solvents investigated (entries 3–6). A quantitative yield of the product with a *cis*-fused stereogenic center was obtained when the reaction time was extended to 15 h (Table 1, entry 10). Control experiments indicated no transformation in the dark or under a nitrogen atmosphere (Table 1, entries 7 and 8), suggesting that oxygen and visible light are essential for this OCCR. Moreover, OCCR exhibited a light source-dependent behavior (Table 1, entry 9). Next, we investigated the effect of structural defects in the framework on the reaction. Introducing defects into the COF efficiently improved the product yield (Table 1, entries 11–14). COF-HNU30-10 quantitatively synthesized tetrahydroquinoline **3a** with a remarkable yield of >99.9%. Compared with COF-HNU30-0 without any structural defect, the catalytic efficiency of COF-HNU30-10 increased by a factor of two, with the yield of the product increasing from 49% to >99.9%. However, the photocatalytic activity gradually decreased with increasing defects (*x* = 20, 30). Thus, only suitable structural defects in the framework can maximize the catalytic performance of semiconductor materials. In addition, we compared the catalytic efficiency of the COF with that of other heterogeneous catalysts. As seen in Table 2 and Fig. S29,† the product yield with COF-HNU30-10 was the highest among these catalysts, even higher than that obtained with Pt and Ru-based heterogeneous catalysts.[33,39] These results suggest that COF-HNU30-10 is a highly efficient photocatalyst for the OCCR of *N*,*N*-dimethylanilines with maleimides.

To better understand the different photocatalytic activities of COF-HNU30-10 and COF-HNU30-0, their optical and electronic properties were systematically investigated to reveal the key differences in their band structures and charge carrier behavior. Compared to the UV-visible diffuse reflectance spectra (UV/Vis DRS) of COF-HNU30-0, the corresponding spectra of COF-HNU30-10 exhibit a large red-shift (30 nm) of the optical adsorption edge at 645 nm (Fig. 3A), indicating that the unique defective structure promoted light-harvesting ability. The band gap energies of the two photocatalysts were estimated to be 1.89 and 1.95 eV for COF-HNU30-10 and COF-HNU30-0, respectively (inset of Fig. 3A). The narrow band gap energy of COF-HNU30-10 is beneficial for improving the electrical performance. The conduction band energies calculated from the Mott–Schottky (M–S) curve are approximately −0.91 and −0.61 V for COF-HNU30-10 and COF-HNU30-0, respectively (Fig. 3B and Fig. S25, S26†). Both COFs exhibited positive slopes, which is a typical characteristic of n-type semiconductors.[42] So, the valence band potentials for COF-HNU30-10 and COF-HNU30-0 are determined to be 0.98 and 1.34 eV, respectively, corresponding to the band structure alignments in Fig. S27.† In particular, we find that COF-HNU30-10 has better reduction properties than COF-HNU30-0 (Fig. S27†); therefore, COF-HNU30-10 is more efficient at reducing dioxygen to superoxide radicals, which is a key active species in the

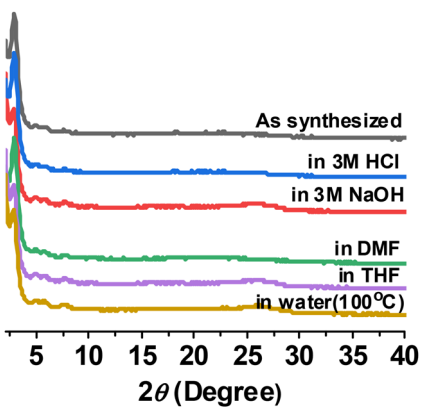

Fig. 2 PXRD patterns of COF-HNU30-10 after various treatments for 3 days.

Table 2 Comparison of the catalytic efficiency of COF-HNU30-10 with that of other heterogeneous catalysts

Catalyst	Metal additive	Time/h	Yield/%
COF-HNU30-10	—	15	>99.9
H_2P-Bph-COF	—	14	72 [13]
P-BBT-10	—	24	88 [40]
UIO-66-TDP	—	12	87 [41]
LTG-NiRu	[Ru]	12	99 [39]
COF-UARK-49	[Pt]	3.5	87 [33]

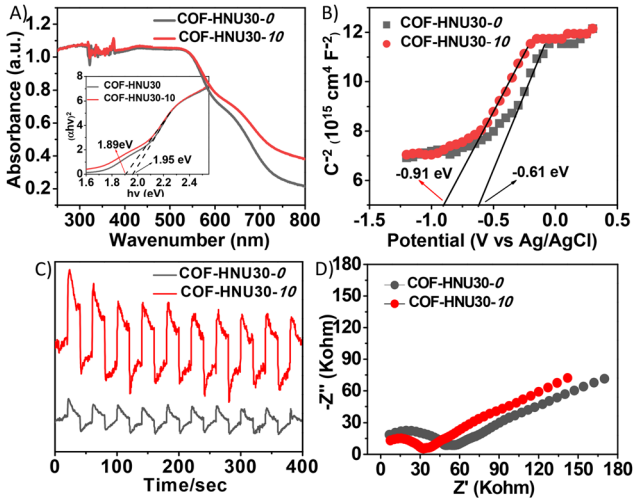

Fig. 3 UV-visible diffuse reflectance spectra with the Tauc plot (A), Mott–Schottky curve (B), transient photocurrent responses (C), and electrochemical impedance spectroscopy (EIS) Nyquist plots (D) of COF-HNU30-0 and COF-HNU30-10.

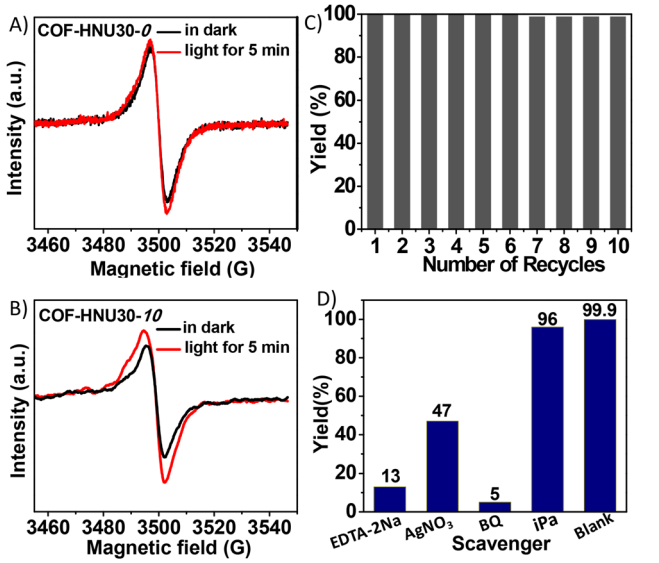

Fig. 4 (A and B) EPR conduction band e-signals of COF-HNU30-0 and COF-HNU30-10 under dark and light conditions for 5 min. (C and D) Recyclability and quenching experiments of COF-HNU30-10.

photocatalytic OCCR. Therefore, COF-HNU30-0 shows lower photocatalytic performance than COF-HNU30-10 in the OCCR.

The separation efficiencies of the photogenerated electrons–holes of COF-HNU30-10 and COF-HNU30-0 were further investigated. Transient photocurrent measurements reveal that COF-HNU30-10 has a higher photocurrent response than COF-HNU30-0 (Fig. 3C). The higher the intensity of photocurrent, the more the photogenerated electrons, which supports more efficient charge separation in COF-HNU30-10.[43] This judgment was supported by the electrochemical impedance spectroscopy (EIS) results (Fig. 3D), where COF-HNU30-10 shows a smaller radius, manifesting lower charge transfer resistance.[44] Steady-state fluorescence spectroscopy and electron paramagnetic resonance spectrometry (EPR) were conducted to further verify the charge separation efficiency in the activity of COF-HNU30-10 and COF-HNU30-0. COF-HNU30-10 exhibited a lower fluorescence intensity than COF-HNU30-0 (Fig. S28†), thereby strongly suppressing radiative exciton recombination. The photogenerated holes were detected using an *in situ* EPR spectrometer. Compared to the dark conditions, both COFs responded in the form of free-radical signals after 5 min of illumination under excitation by the same light source. COF-HNU30-10 displays a higher signal intensity after illumination (Fig. 4A and B), demonstrating a higher carrier concentration.[45] Combined with the above results, the boosted charge transfer and separation of electrons–holes caused by the introduction of moderate defects in the framework improve photocatalytic activity.

The applicability of COF-HNU30-10 as a heterogeneous photocatalyst for synthesizing tetrahydroquinolines was further tested; the results are listed in Table 3. Initially, various maleimides were investigated. Maleimides bearing alkyl- or aryl-substituents could effectively synthesize the desired tetrahydroquinolines, offering excellent yields. Similarly, *N*,*N*-dimethylanilines with electron-withdrawing or electron-donating substituents can also react with maleimides to obtain the desired products in high yields. However, steric effects considerably influence the photocatalytic OCCR. For example, only a moderate yield of **3p** was achieved in the reaction system. Moreover, the structures of all known compounds were characterized using melting points and ^{1}H and ^{13}C NMR spectra, which are consistent with the reported literature.[6,16a,18,39] Other compounds were characterized using melting points, HRMS, and ^{1}H and ^{13}C NMR spectra, respectively (see the details in the ESI†).

In industrial catalytic processes, apart from catalytic performance, the recyclability and economic feasibility of materials are also considered. COF-HNU30-10 exhibited the highest catalytic efficiency among the reported heterogeneous photocatalysts. Moreover, COF-HNU30-10 could be reused for at least 10 cycles without a substantial decline in photocatalytic activity (Fig. 4C and S30, S31†). Economic feasibility influences the implementation of COFs on an industrial scale and is closely related to the cost and scalability of the catalyst. The synthesis of COFs relies on conventional solvothermal methods at high temperatures with complex operations that are not amenable to large-scale production, resulting in prohibitively high production costs. Thus, COF-HNU30-10 was prepared using three reagents that can be synthesized from inexpensive and readily available starting materials: aminobenzonitrile ($64.5 per kg) and hydroquinone ($12.1 per kg). Most importantly, COF-HNU30-10 can be synthesized on a gram scale at room temperature, reducing energy consumption and production costs. In summary, the excellent catalytic performance, high stability, and cost-effectiveness of COF-HNU30-10 make it a promising catalyst for environmentally-friendly synthesis of tetrahydroquinoline derivatives.

Table 3 The substrate scope for the photocatalytic synthesis of tetrahydroquinolines[a,b]

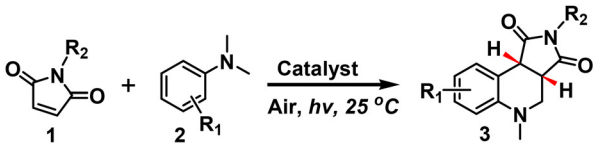

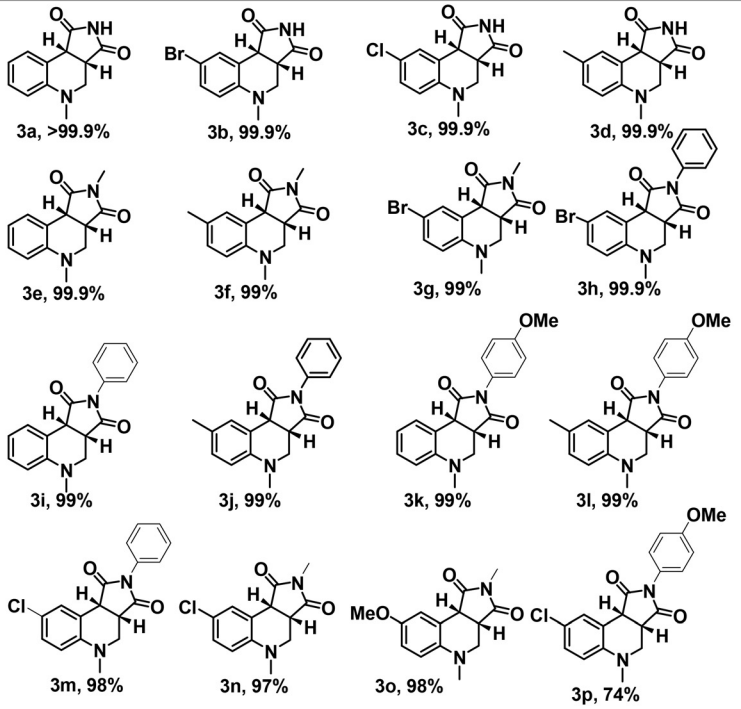

[a] Reaction conditions: 0.25 mmol **1**, 0.5 mmol **2**, 5 mg COF-HNU30-10, 2 mL DMF, ambient air atmosphere, room temperature, and irradiation using a 20 W LED white light source. [b] Using 1,3,5-trimethoxybenzene as an internal standard, yield was monitored by ^{1}H NMR.

To gain further insight into the photocatalytic mechanism of the OCCR, we conducted controllable experiments using COF-HNU30-10 as the catalyst and maleimide **1a** and *N*,*N*-dimethylaniline **2b** as model substrates. As shown in Fig. 4D, the product yield linearly decreases when using ethylenediaminetetraacetic acid disodium salt (EDTA-2Na) as the hole scavenger. Adding $AgNO_3$ as an electron scavenger also decreases the catalytic efficiency of COF-HNU30-10. However, using benzoquinone (BQ) to trap the superoxide radicals nearly halted the reaction. In contrast, adding 2-propanol, a hydroxyl radical scavenger, did not significantly reduce the catalytic efficiency of COF-HNU30-10. These results indicate that holes, electrons, and superoxide radicals are the key active species in the photocatalytic synthesis of tetrachloroquinolines.

Based on the aforementioned results, Fig. S32† presents a similar mechanism as that proposed in ref. 39 for the photocatalytic synthesis of tetrahydroquinolines with COF-HNU30-10. First, under light irradiation, the ground-state electrons in COF-HNU30-10 are excited, generating electron vacancies (holes) within the material. The excited-state COF-HNU30-10* captures the electrons from **2a**, forming electron–hole pairs, and reduces the oxygen in the air to superoxide radicals. The electron-deficient radical cation **2a′** loses a proton (H^+) in the presence of superoxide radicals, generating the active intermediate **2a″**. Intermediate **2a″**, with oxidative properties, induces the oxidation of the carbon–carbon double bond within **1a**, yielding intermediate **3**. However, intermediate **3** undergoes intramolecular cyclization owing to instability, generating the more stable intermediate **4**. In the presence of superoxide radicals, intermediate **4** loses an electron and a proton, ultimately reaching the stable structure **5**.

Conclusions

This study presents a unique imine-based COF-HNU30-10 catalyst with good stability and a high structural defect density in the framework for the selective OCCR of *N*,*N*-dimethylanilines with maleimides. Benefiting from the effective electron–hole separation, low charge transfer resistance, and increased charge lifetime, an excellent photocatalytic activity has been achieved by COF-HNU30-10 with the introduction of moderate defects in the framework. The catalytic efficiency of COF-HNU30-10 in the OCCR was higher than that observed for

non-defective COF-HNU30-0. The product yield increased from 49% with COF-HNU30-0 to >99.9% with COF-HNU30-10. In addition, the high stability and cost-effectiveness of COF-HNU30-10 make it a promising catalyst for environmentally-friendly synthesis of tetrahydroquinolines. This work suggests valuable guidelines for designing metal-free heterogeneous catalysts to synthesize tetrahydroquinolines quantitatively. Moreover, it offers a new perspective for developing novel visible-light-responsive COFs with balanced catalytic performance, stability and cost-effectiveness to promote their industrial implementation for significant organic synthesis.

Conflicts of interest

There are no conflicts to declare.

Acknowledgements

This work is supported financially by the National Natural Science Foundation of China (no. 22073024) and the Henan Provincial Department of Science and Technology Research Project (222102320153). The authors are thankful for the support from the Shiyanjia Lab (**https://www.shiyanjia.com**) for the EPR analysis. The authors are also thankful for the support by the High Performance Computing Center of Henan Normal University for this work.

Notes and references

1 J. P. Michael, *Nat. Prod. Rep.*, 2007, **24**, 223.
2 D. V. Kravchenko, Y. A. Kuzovkova, V. M. Kysil, S. E. Tkachenko, S. Maliarchouk, I. M. Okun, K. V. Balakin and A. V. Ivachtchenko, *J. Med. Chem.*, 2005, **48**, 3680–3693.
3 K. Grychowska, G. Satała, T. Kos, A. Partyka, E. Colacino, S. Chaumont-Dubel, X. Bantreil, A. Wesołowska, M. Pawłowski, J. Martinez, P. Marin, G. Subra, A. J. Bojarski, F. Lamaty, P. Popik and P. Zajdel, *ACS Chem. Neurosci.*, 2016, **7**, 972–983.
4 M. Balasubramanian, in *Pyridines: From Lab to Production*, ed. E. F. V. Scriven, Academic Press, Oxford, 2013, pp. 413–458.
5 A. K. Yadav and L. D. S. Yadav, *Tetrahedron Lett.*, 2016, **57**, 1489–1491.
6 (*a*) J. Hu, S. Wang, B. Li and A. Lei, *Org. Lett.*, 2023, **25**, 1252–1256; (*b*) M. Nishino, K. Hirano, T. Satoh and M. Miura, *J. Org. Chem.*, 2011, **76**, 6447–6451; (*c*) J. Y. Hwang, A. Y. Ji, S. H. Lee and E. Kang, *Org. Lett.*, 2020, **22**, 16–21; (*d*) C. Hsu and H. Sunden, *Org. Lett.*, 2018, **20**, 2051–2054; (*e*) Z. Song and A. P. Antonchick, *Tetrahedron*, 2016, **72**, 7715–7721; (*f*) J. Tang, G. Grampp, Y. Liu, B.-X. Wang, F.-F. Tao, L.-J. Wang, X.-Z. Liang, H.-Q. Xiao and Y.-M. Shen, *J. Org. Chem.*, 2015, **80**, 2724–2732.
7 N. Sakai, S. Matsumoto and Y. Ogiwara, *Tetrahedron Lett.*, 2016, **57**, 5449–5452.
8 (*a*) S. Firoozi, M. Hosseini-Sarvari and M. Koohgard, *Green Chem.*, 2018, **20**, 5540–5549; (*b*) X.-L. Yang, J.-D. Guo, T. Lei, B. Chen, C.-H. Tung and L.-Z. Wu, *Org. Lett.*, 2018, **20**, 2916–2920.
9 A. K. Yadav and L. D. S. Yadav, *Tetrahedron Lett.*, 2017, **58**, 552–555.
10 J. Mateos, F. Rigodanza, A. Vega-Peñaloza, A. Sartorel, M. Natali, T. Bortolato, G. Pelosi, X. Companyó, M. Bonchio and L. Dell'Amico, *Angew. Chem., Int. Ed.*, 2019, **59**, 1302–1312.
11 A. M. Ranieri, L. K. Burt, S. Stagni, S. Zacchini, B. W. Skelton, M. I. Ogden, A. C. Bissember and M. Massi, *Organometallics*, 2019, **38**, 1108–1117.
12 X. Ju, D. Li, W. Li, W. Yu and F. Bian, *Adv. Synth. Catal.*, 2012, **354**, 3561–3567.
13 C. Wu, X. Li, M. Shao, J. Kan, G. Wang, Y. Geng and Y.-B. Dong, *Chin. Chem. Lett.*, 2022, **33**, 4559–4562.
14 T. P. Nicholls, G. E. Constable, J. C. Robertson, M. G. Gardiner and A. C. Bissember, *ACS Catal.*, 2015, **6**, 451–457.
15 G. Perumal, M. Kandasamy, B. Ganesan, K. Govindan, H. Sathya, M.-Y. Hung, G. Chandru Senadi, Y.-C. Wu and W.-Y. Lin, *Tetrahedron*, 2021, **80**, 131891.
16 (*a*) A. Runemark and H. Sundén, *J. Org. Chem.*, 2022, **87**, 1457–1469; (*b*) T. Mandal, S. Das and S. De Sarkar, *Adv. Synth. Catal.*, 2019, **361**, 3200–3209.
17 J. Li, W. Bao, Y. Zhang and Y. Rao, *Org. Biomol. Chem.*, 2019, **17**, 8958–8962.
18 J.-T. Guo, D.-C. Yang, Z. Guan and Y.-H. He, *J. Org. Chem.*, 2017, **82**, 1888–1894.
19 A. P. Côté, A. I. Benin, N. W. Ockwig, M. O'Keeffe, A. J. Matzger and O. M. Yaghi, *Science*, 2005, **310**, 1166–1170.
20 A. Jati, K. Dey, M. Nurhuda, M. A. Addicoat, R. Banerjee and B. Maji, *J. Am. Chem. Soc.*, 2022, **144**, 7822–7833.
21 E. Jin, Z. Lan, Q. Jiang, K. Geng, G. Li, X. Wang and D. Jiang, *Chem*, 2019, **5**, 1632–1647.
22 T.-Y. Yu, Q. Niu, Y. Chen, M. Lu, M. Zhang, J.-W. Shi, J. Liu, Y. Yan, S.-L. Li and Y.-Q. Lan, *J. Am. Chem. Soc.*, 2023, **145**, 8860–8870.
23 A. Basak, S. Karak and R. Banerjee, *J. Am. Chem. Soc.*, 2023, **145**, 7592–7599.
24 S. Bi, Z. Zhang, F. Meng, D. Wu, J. Chen and F. Zhang, *Angew. Chem., Int. Ed.*, 2021, **61**, e202111627.
25 D. Chen, W. Chen, G. Zhang, S. Li, W. Chen, G. Xing and L. Chen, *ACS Catal.*, 2021, **12**, 616–623.
26 H. Chen, H. S. Jena, X. Feng, K. Leus and P. V. D. Voort, *Angew. Chem., Int. Ed.*, 2022, **61**, e202204938.
27 Y. Fan, D. W. Kang, S. Labalme, J. Li and W. Lin, *Angew. Chem., Int. Ed.*, 2023, **62**, e202218908.
28 J. Wang, X.-X. Tian, L. Yu, D. J. Young, W.-B. Wang, H.-Y. Li and H.-X. Li, *J. Mater. Chem. A*, 2021, **9**, 25474–25479.
29 L. Stegbauer, K. Schwinghammer and B. V. Lotsch, *Chem. Sci.*, 2014, **5**, 2789–2793.

30 J. Zhao, G. Guo, D. Wang, H. Liu, Z. Zhang, L. Sun, N. Ding, Z. Li and Y. Zhao, *Green Chem.*, 2023, **25**, 3103–3110.
31 Z. Fu, X. Wang, A. M. Gardner, X. Wang, S. Y. Chong, G. Neri, A. J. Cowan, L. Liu, X. Li, A. Vogel, R. Clowes, M. Bilton, L. Chen, R. S. Sprick and A. I. Cooper, *Chem. Sci.*, 2020, **11**, 543–550.
32 H. Chen, W. Liu, A. Laemont, C. Krishnaraj, X. Feng, F. Rohman, M. Meledina, Q. Zhang, R. V. Deun, K. Leus and P. V. D. Voort, *Angew. Chem., Int. Ed.*, 2021, **60**, 10820–10827.
33 Z. Almansaf, J. Hu, F. Zanca, H. R. Shahsavari, B. Kampmeyer, M. Tsuji, K. Maity, V. Lomonte, Y. Ha, P. Mastrorilli, S. Todisco, M. Benamara, R. Oktavian, A. Mirjafari, P. Z. Moghadam, A. R. Khosropour and H. Beyzavi, *ACS Appl. Mater. Interfaces*, 2021, **13**, 6349–6358.
34 Y. Wang, Y. Shi, Z. Li, H. Wang, J. Qiu, X. Xuan and J. Wang, *ACS Sustainable Chem. Eng.*, 2022, **10**, 12457–12465.
35 Z. Guo, H. Wu, Y. Chen, S. Zhu, H. Jiang, S. Song, Y. Ren, Y. Wang, X. Liang, G. He, Y. Li and Z. Jiang, *Angew. Chem., Int. Ed.*, 2022, **61**, e202210466.
36 J. Qiu, C. Xu, X. Xu, Y. Zhao, Y. Zhao, Y. Zhao and J. Wang, *Angew. Chem., Int. Ed.*, 2023, **62**, e202300459.
37 S. Yang, Z. Chen, L. Zou and R. Cao, *Adv. Sci.*, 2023, **10**, 2304697.
38 Y. Zhao, Y. Zhao, C. Wu, J. Qiu, H. Wang, Z. Li, Y. Zhao and J. Wang, *Chem – Eur. J.*, 2021, **27**, 9391–9397.
39 D. Bai, J. Qiu, J. Li, S. Zhou, X. Cui, X. Tang, Y. Tang, W. Liu and B. Chen, *ACS Appl. Mater. Interfaces*, 2023, **15**, 30320–30331.
40 Z. J. Wang, S. Ghasimi, K. Landfester and K. A. I. Zhang, *Adv. Synth. Catal.*, 2016, **358**, 2576–2582.
41 C. Li, H. Zhang, X. Wang, Q.-Y. Li, X. Zhao and X.-J. Wang, *RSC Adv.*, 2022, **12**, 1638–1644.
42 X. Lan, X. Liu, Y. Zhang, Q. Li, J. Wang, Q. Zhang and G. Bai, *ACS Catal.*, 2021, **11**, 7429–7441.
43 Z. Lu, R. Zhao, H. Yang, X. Fu, Y. Zhao, L. Xiao and L. Hou, *Angew. Chem., Int. Ed.*, 2022, **61**, e202208898.
44 Y. Wang, F. Huang, W. Sheng, X. Miao, X. Li, X.-K. Gu and X. Lang, *Appl. Catal., B*, 2023, **338**, 123070.
45 X. Li, Y. Wang, F. Zhang and X. Lang, *Appl. Catal., B*, 2024, **340**, 123190.